Substrate-Induced Solvent Intercalation for Stable Graphene Doping

Hyun Ho Kim,[†] Jae Won Yang,[‡] Sae Byeok Jo,[†] Boseok Kang,[†] Seong Kyu Lee,[†] Hyojin Bong,[†] Geunsik Lee,[‡] Kwang S. Kim,[‡] and Kilwon Cho[†,*]

[†]Department of Chemical Engineering and [‡]Center for Superfunctional Materials, Pohang University of Science and Technology, Pohang 790-784, Korea

ABSTRACT Here, we report a substrate-induced intercalation phenomenon of an organic solvent at the interface between monolayer graphene and a target substrate. A simple dipping of the transferred chemical vapor deposition (CVD)-grown graphene on the SiO_2 substrate into chloroform ($CHCl_3$, CF), a common organic solvent, induces a spontaneous formation of CF clusters beneath the basal plane of the graphene as well as inside the wrinkles. The microscopic and spectroscopic observations showed the doping behavior of monolayer graphene, which indicates the adsorption of CF to monolayer graphene. Interestingly, the intercalated organic solvent showed remarkable stability for over 40 days under ambient conditions. To reveal the underlying mechanism of the stable solvent intercalation, desorption energy of CF molecules at the graphene/substrate interface was measured using Arrhenius plots of the conductance change upon time and temperature. Two stages of solvent intercalations with high desorption energies (70 and 370 meV) were observed along with the consecutive shrinkage of the solvent clusters at the basal plane and the wrinkles, respectively. Moreover, the theoretical calculation based on density functional theory (DFT) also shows the strong intercalation energy of CF between monolayer graphene and the SiO_2 substrate, which results from the stabilization of the graphene−SiO_2 interactions. Furthermore, the thermal response of the conductance could be utilized to maintain a certain degree of p-doping of monolayer graphene, which provides the facile, sustainable, and controllable large-area doping method of graphene for future generation of printed flexible electronics.

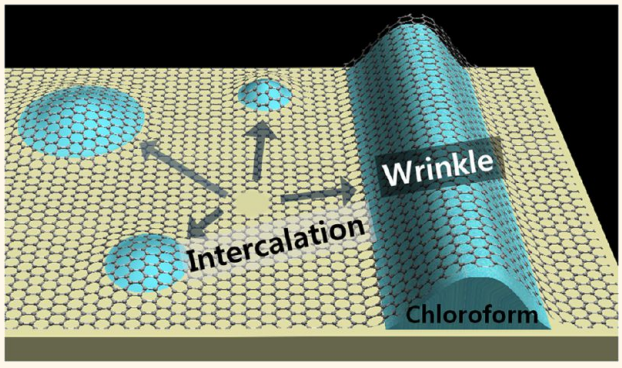

KEYWORDS: graphene · substrate-induced solvent intercalation · molecular doping · graphene wrinkle

Graphene, a fully conjugated two-dimensional hexagonal carbon molecule lattice, has attracted much attention because of its excellent mechanical,[1] thermal,[2] optical,[3,4] and electrical properties.[5−8] Among diverse intriguing properties of graphene, the high transmittance,[9] low sheet resistance,[10] and tunability of the work function[11,12] have been used to fabricate high-performance soft electronic devices such as organic field effect transistors (OFETs),[13−15] organic photovoltaics (OPVs),[16] and organic light-emitting diodes (OLEDs).[17,18] To enhance the performance of devices using graphene electrodes, doping can be applied; using doping, the work function and sheet resistance of graphene can be controlled.[11,12] Recently, a variety of doping methods have been developed, including substitutional doping,[19] electrochemical doping,[20] and molecular contact doping.[12,21−26] Molecular contact doping was shown to be suitable for soft electronic devices[12] because defects were not generated during the doping process.[27] Various dopant molecules have been used in this method, including aromatic molecules,[21,28] self-assembled monolayers (SAM),[12,22] metal nanoparticles,[26] and acids.[10] A simple, stable, reproducible, controllable, low-temperature, and large-scale method that does not sacrifice transmittance is a desirable goal of doping.

Herein, we report a spontaneous substrate-induced intercalation of chloroform ($CHCl_3$, CF) at the graphene/SiO_2 interface and develop a p-doping of graphene using this result. The solvent doping effect of graphene was reported before, but it dealt

* Address correspondence to kwcho@postech.ac.kr.

Received for review September 13, 2012 and accepted January 24, 2013.

Published online January 31, 2013
10.1021/nn306012p

with only the case when graphene is immersed in organic solvents.[29] We suggest that the solvent intercalation doping achieves reproducible, stable, and strong p-doping in the absence of a barrier film because solvent is spontaneously intercalated at the graphene/SiO_2 interface; note that stable doping with acids requires the presence of a protective barrier film because of the instability of the doping agents at atmospheric pressure.[30] Here we show where the CF molecules are intercalated and how strongly they interact with graphene. Furthermore, we suggest that the doping level can be modulated by controlling the desorption of intercalated CF clusters.

RESULTS AND DISCUSSION

Monolayer graphene grown on a copper foil was transferred onto a SiO_2 (300 nm)/Si wafer, and the poly(methyl methacrylate) (PMMA) supporting layer on the graphene was then removed by using acetone or CF. Both photography and field emission scanning electron microscopy (FESEM) images confirmed the successful transfer of the chemical vapor deposition (CVD)-grown graphene from the copper foil to the target SiO_2/Si substrate (Supporting Information, Figure S1b,c). The removal of PMMA with acetone did not induce the doping of graphene; in contrast, when CF was used, the graphene was significantly doped. When the PMMA/graphene/SiO_2/Si sample was immersed in CF for 1 h, the PMMA was dissolved, and the graphene was simultaneously doped (Supporting Information, Figure S1a). To investigate the effects of the doping of graphene with CF, the conductance and V_G measurements, Raman spectroscopy, and ultraviolet photoelectron spectroscopy (UPS) experiments were performed, as shown in Figure 1.

The gate-voltage-dependent conductance in graphene FETs indicates the type and magnitude of the graphene doping. For undoped graphene samples where the PMMA was removed using acetone, the Dirac voltage was 10 V. The low p-doping of the graphene might have been due to the presence of PMMA residues and/or adsorbates on the SiO_2 substrate. On the other hand, only the hole conductance was observed, and the Dirac voltage increased by over 10 times when the graphene sample was dipped in CF to remove the PMMA, as shown in Figure 1a. These results were reproducible, and therefore, the significant p-doping of graphene with CF was confirmed. Considering that the electrical measurements were performed under high vacuum conditions ($\sim 10^{-5}$–10^{-6} Torr), the effects of the doping of graphene with CF were quite substantial. In addition, the doping remained stable for more than 40 days at room temperature and atmospheric pressure, as shown in Figure 1b. Meanwhile, the hole mobility was measured to be around 3500 $cm^2/V \cdot s$, which was calculated in the linear regime. This is a relatively high value compared to other doping methods using graphene (SAM doping of CVD graphene, $\sim$1800 $cm^2/V \cdot s$;[12] $AuCl_3$ doping, 1735 $cm^2/V \cdot s$;[31] CYTOP doping, 810 $cm^2/V \cdot s$[25]).

Raman spectroscopy measurements were also performed to confirm the effects of doping. Raman spectroscopy is a nondestructive technique and is useful for identifying the effects of doping,[20] as well as the quality of the graphene.[32] Figure 1c illustrates the changes in the Raman spectra for monolayer graphene after CF doping. The D band (1350 cm^{-1}) did not appear after doping, indicating that defects were not activated under CF doping. In the Raman spectrum of undoped graphene, the G and 2D bands were located at 1588 and 2679 cm^{-1}, respectively, and the I_G/I_{2D} ratio was 0.45. This result was similar to the reported value for CVD-grown graphene on the SiO_2 surface.[33] However, the Raman spectrum for the CF-doped graphene showed blue shifts for both G and 2D bands, at 1596 and 2689 cm^{-1}, and the full width at half-maximum (fwhm) of the G band was decreased from 18 to 13 cm^{-1}. In addition, the I_G/I_{2D} ratio increased to 0.7. These results are consistent with the stiffening and sharpening of the G band after doping due to the breakdown of the adiabatic Born–Oppenheimer approximation and to blocking of the channel for the decay of phonons into electron–hole pairs, respectively.[34]

The effects of doping of graphene with CF were also confirmed by measuring the work function of the graphene. Figure 1d shows the UPS spectra of undoped and CF-doped graphene. SiO_2(300 nm)/n^+-Si wafer was used, and carbon tape/tantalum foil was connected between sample holder and the graphene surface for prevention of electron charging. The work function was calculated using the following equation:

$$\Phi = \hbar\omega - |E_{SEC} - E_{FE}| \quad (1)$$

where $\hbar\omega$ = 130 eV, E_{SEC} is the onset of the secondary emission, and E_{FE} is the Fermi edge (−125.65 eV) under a sample bias of −20 V. The work functions of undoped and CF-doped graphene were measured to be 4.61 and 5.19 eV, respectively. The slight increase in the measured work function for the undoped graphene compared with the theoretical value of 4.42 eV[35] was likely due to uncontrollable graphene doping from the charged impurities on the SiO_2 substrate.[6] The abrupt increase (0.58 eV) in the work function of the graphene was caused by the p-doping with CF. The p-doping down-shifted the Fermi level relative to the Dirac point, thereby increasing the density of hole carriers and the work function of the graphene. The increased hole carrier density in the CF-doped graphene decreased the sheet resistance of the graphene electrode, from 630 to 300 ohm/sq. However, the transmittance (T, %) of the graphene film at 550 cm^{-1} remained at 97.7%, regardless of the presence or absence of CF doping, as shown in Figure 1e. This is one of the most important

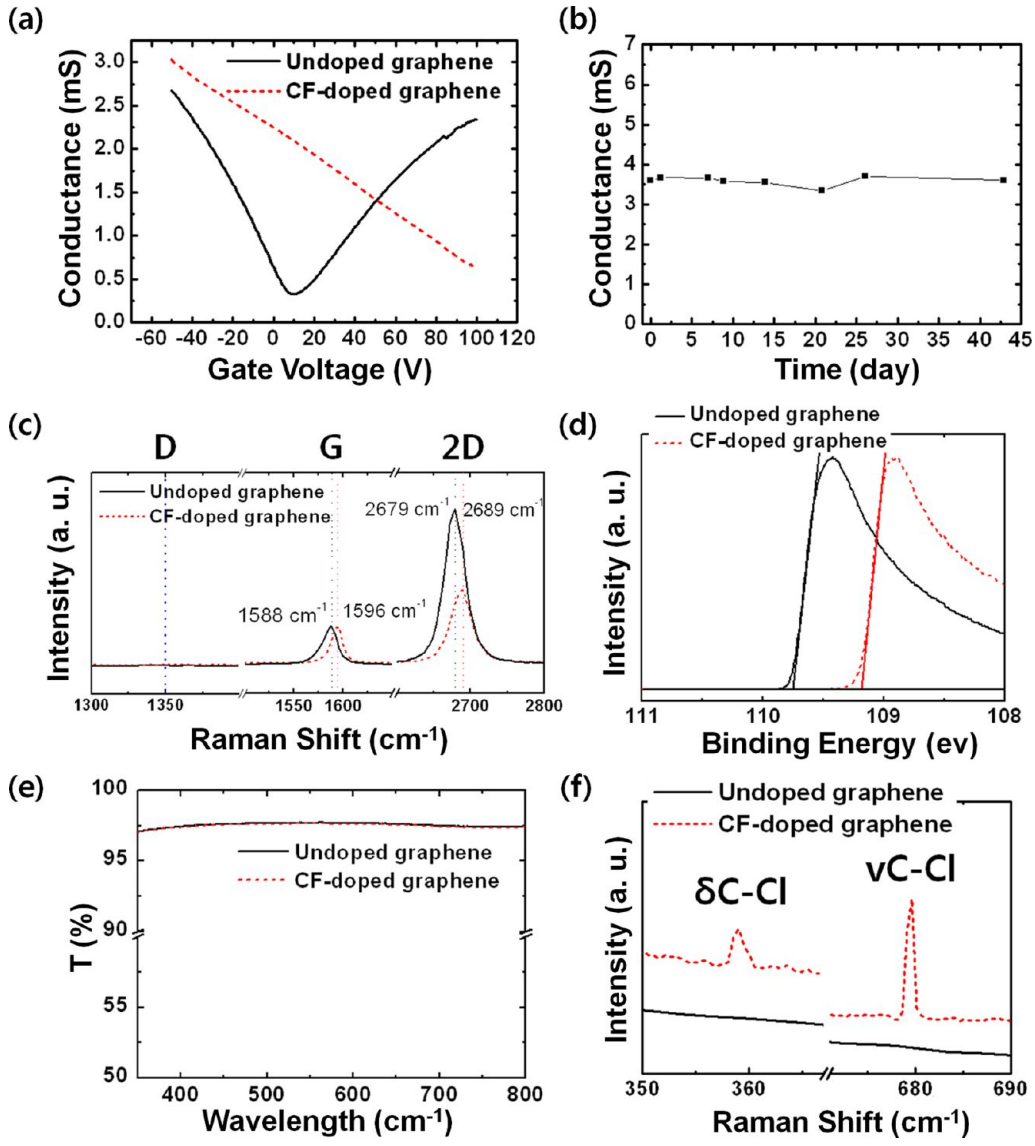

Figure 1. (a) Conductance of graphene FET as a function of V_G. (b) Change in the conductance as a function of time at atmospheric pressure and room temperature. (c) Raman spectra of the undoped and CF-doped graphene film. (d) UPS spectra, (e) UV−vis spectra, and (f) Raman spectra showing the C−Cl vibrational modes of CF. The black solid line and red dashed line indicate undoped and CF-doped graphene, respectively.

advantages of the solvent doping process over other doping methods that sacrifice transmittance.[26]

To identify the presence of the CF in the doped graphene directly, Raman spectroscopy measurements were performed on undoped and CF-doped graphene samples, as shown in Figure 1f. The CF-doped graphene exhibited vibration modes, including deformation (δ_{C-Cl}, 359 cm^{-1}) and stretching (ν_{C-Cl}, 679 cm^{-1}), even after 5 days of storage under atmospheric conditions. However, these peaks were absent for the undoped graphene. In addition, X-ray photoelectron spectroscopy (XPS) was also performed to prove the presence of CF. The result shows that the Cl 2p peak was observed even in ultrahigh vacuum and then 1.39×10^{14} #/cm^2 of CF molecules was contained in CF-doped graphene (Supporting Information, Figure S2). It can therefore be concluded that adsorbed CF was responsible for the observed doping behaviors of the graphene. Meanwhile, the doping efficiency of the CF molecule can be calculated from CF concentration and charge carrier density in CF-doped graphene. The relation between Dirac point and charge carrier density was expressed by the following equation.[36]

$$E_D = \hbar V_F \sqrt{\pi n} \quad (2)$$

where $V_F = 1.1 \times 10^6$ m/s and n = charge carrier density. Since the work function of CF-doped graphene was 5.19 eV, charge carrier density was calculated to be 3.59×10^{13} #/cm^2 from the above equation. Considering charge concentration of the undoped graphene (2.19×10^{12} #/cm^2), we found that 3.37×10^{13} #/cm^2 of holes was induced by CF molecules, and one atom of

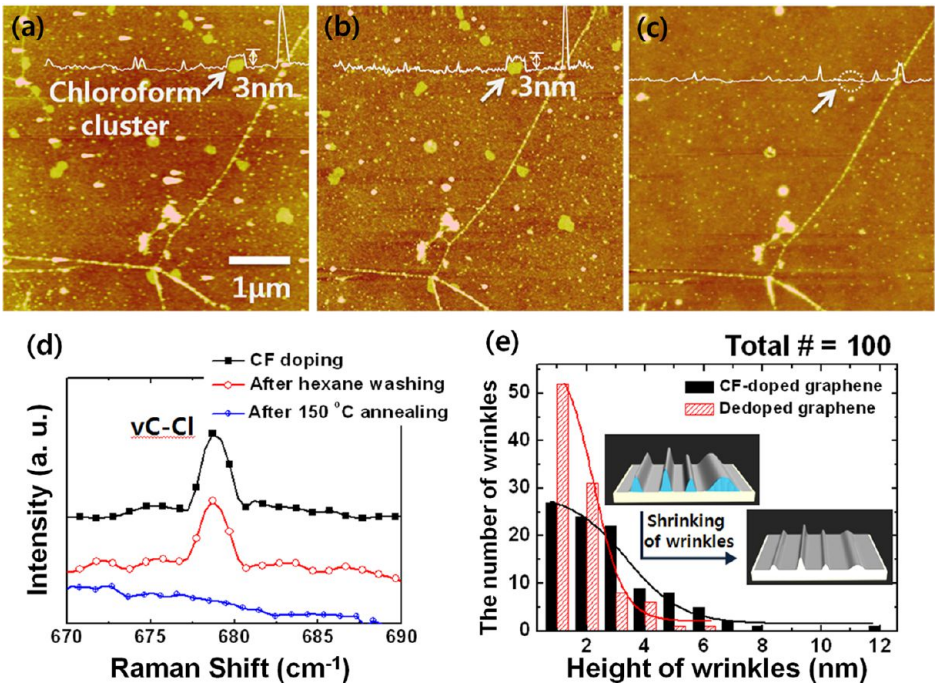

Figure 2. Changes in the AFM images of the graphene surface (a) after immersion in CF for 1h, then (b) after drying in vacuum at room temperature for 12 h, and finally (c) after thermal annealing at 150 °C for 12 h. The scan sizes were 5 μm × 5 μm. (d) Changes in the Raman spectra for CF-doped graphene after rapid hexane washing and 150 °C annealing. (e) Height distribution of wrinkles in CF-doped and undoped graphene. The inset image shows a schematic drawing of the changes in the dimensions of the wrinkles.

CF induces 0.24 holes per CF molecule. This doping efficiency was an average value because CF intercalants consist of a multilayer, which means that the degree of charge transfer is dominantly affected by the nearest CF layer contacted on graphene.

Atomic force microscopy (AFM) images were taken to identify the location of the CF adsorbates, as shown in Figure 2a−c. Sequential AFM images were taken at the same site, after specific environmental treatment; this consisted of dipping for 1 h in CF (Figure 2a), followed by 12 h in a vacuum chamber (Figure 2b), then annealing at 150 °C for 12 h (Figure 2c). It was shown that CF clusters (white arrow in Figure 2a,b) formed when the sample was immersed in CF and did not disappear even under high vacuum conditions, as shown in Figure 2a,b. However, the clusters were removed (white arrow in Figure 2c) or their size was decreased when the sample was annealed at 150 °C. At this temperature, the PMMA residue could not be removed. Thus, the adsorbed CF clusters, rather than the PMMA residue, were responsible for the change in the height profiles.

Stable doping of graphene with CF is an unexpected phenomenon because the boiling point of CF (61.2 °C at atmospheric pressure) is low enough to allow evaporation at room temperature, and the CF−graphene interaction is governed by weak van der Waals forces. There are two possible scenarios: (i) CF is trapped in the PMMA residues on the graphene surface, and (ii) CF is intercalated at the interface between the graphene and the SiO_2. To examine the feasibility of scenario (i), the PMMA residue was thermally removed at 350 °C for 2 h (instead of removing it in the solvent), and the characteristics of the graphene were examined. After the samples were immersed in CF, the AFM images and Raman spectra showed that CF clusters were generated, and p-doping still occurred (Supporting Information, Figure S4). Thus, it can be concluded that the PMMA residue did not provide the sites for the adsorption of CF. To confirm the validity of scenario (ii), Raman spectroscopy measurement was carried out after rapid hexane washing (Figure 2d). The ν_{C-Cl} intensity was almost unchanged, consistent with scenario (ii); CF adsorbates existed at the interface between graphene and SiO_2, rather than on the surface of the graphene. In addition, we confirmed that the ν_{C-Cl} peak disappeared after 150 °C annealing. We speculate that CF molecules were able to penetrate through defects in the graphene (*i.e.*, point defects or cracks) or through the sides of the graphene layer and then formed inhomogeneous clusters (Figure 2a−c). The formation of an inhomogeneous cluster might be induced by the surface energy mismatch of the two surfaces, that is, a rigid bottom substrate with high surface energy (SiO_2) and flexible top layer with low surface energy (graphene).

The next question was at what sites CF adsorption occurred. Figure 2e shows the height distribution of wrinkles in both CF-doped and dedoped graphene. One hundred such wrinkles were examined. After thermal annealing at 150 °C, the average height of the wrinkles

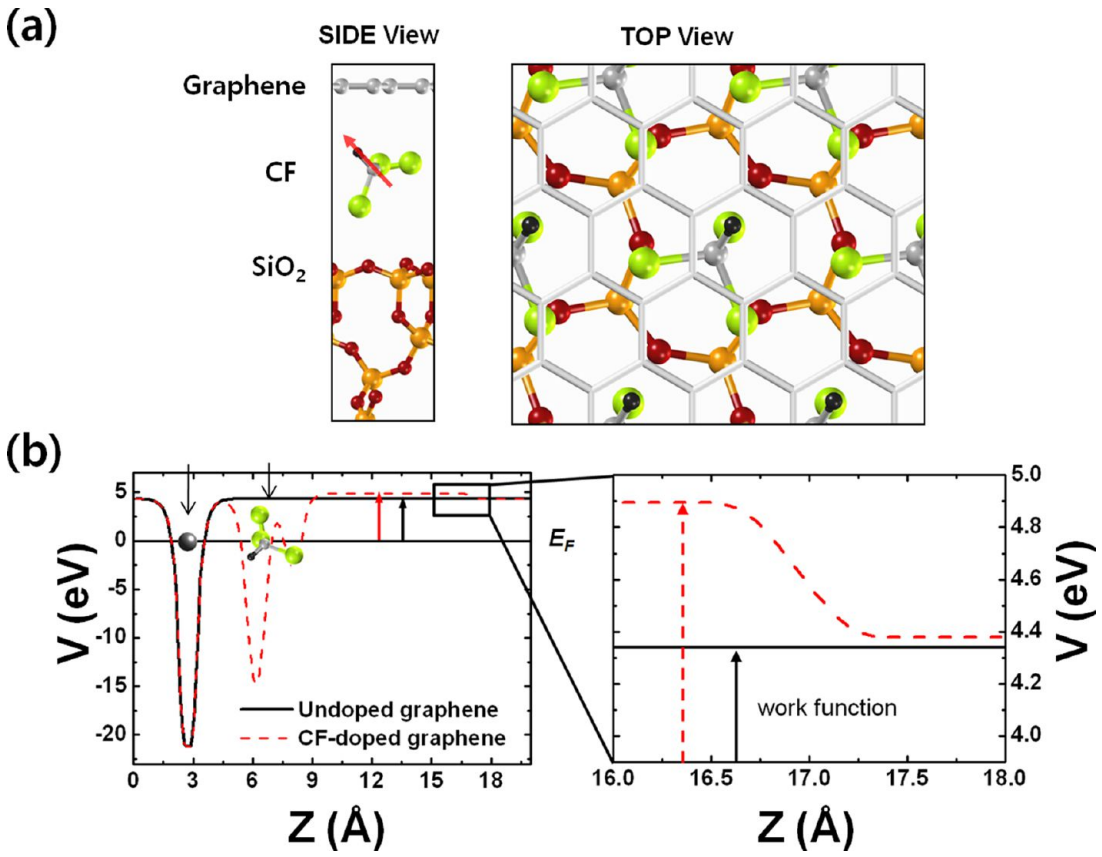

Figure 3. (a) Interfacial structure of the SiO_2-CF-graphene system (gray, C; black, H; green, Cl; red, O; orange, Si). The red arrow plotted in the side view indicates the direction of the CF dipole moment. Chlorine atoms are located at the hollow sites of the six-membered ring of the SiO_2 surface. (b) Plane averaged electrostatic potential of the CF-doped graphene and the undoped graphene. The positions of the graphene and CF layers are indicated together.

decreased from 3.3 ± 1.9 to 2.1 ± 1 nm, and the fwhm of the distribution became narrow. These results are consistent with CF intercalation expanding the wrinkles and CF desorption shrinking them, as shown schematically in the inset of Figure 2e. As well as being trapped in the wrinkles, CF could also be trapped at the interface between the basal plane of the graphene and the SiO_2 substrate. This was confirmed by the removal of the CF clusters with thermal annealing at 150 °C (Figure 2a–c). Another evidence for the intercalation of CF was found by examining the effects of the doping of a suspended graphene layer. Since the suspended graphene had no sites for intercalation, the p-doping effect did not occur after the sample was dipped in CF (Supporting Information, Figure S5).

To explain the observed CF intercalation, we carried out total energy calculations using density functional theory (DFT). As shown in Figure 3a, the system was modeled by a symmetric slab with a lateral unit cell size of eight carbon atoms. The original O-terminated alpha quartz SiO_2(001) surface changed to give a six-membered ring consisting of six Si–O units, where each carbon atom was located on a hollow site.[37] Considering the occupied volume of CF molecule and the available space between graphene and SiO_2, we confirmed that one CF molecule per 2 × 2 graphene cell is appropriated. To analyze the stability, we define the intercalation energy per CF molecule as follows:

$$E_{\text{intercalation}} = -\frac{1}{N_{\text{CF}}}\left(E_{\text{G-CF-SiO}_2} - E_{\text{G-SiO}_2} - N_{\text{CF}}E_{\text{CF}}\right) \quad (3)$$

Here, N_{CF} represents the number of CF molecules intercalated at the interface, and $E_{\text{G-CF-SiO}_2}$, $E_{\text{G-SiO}_2}$, and E_{CF} stand for the total energy of the CF intercalated system, the graphene-on-SiO_2 surface system, and the CF molecule, respectively. We calculated two structures with different dipole moment orientations for the CF inside the graphene–SiO_2 interface: the hydrogen-upward direction (Figure 3a), and the hydrogen-downward direction. On the basis of the calculations, the intercalation energy of the hydrogen-upward CF was 0.28 eV, and that of the hydrogen-downward CF was 0.23 eV. Because the SiO_2 surface layer was positively charged, the upward dipole direction of CF was more energetically stable than the downward one.

We further studied the change in the work function after CF intercalation. Graphene with hydrogen-upward CF molecules but without the SiO_2 substrate was considered in comparison with intrinsic graphene. During calculation, the system consists of a CF(top)/graphene structure because the induced dipole of

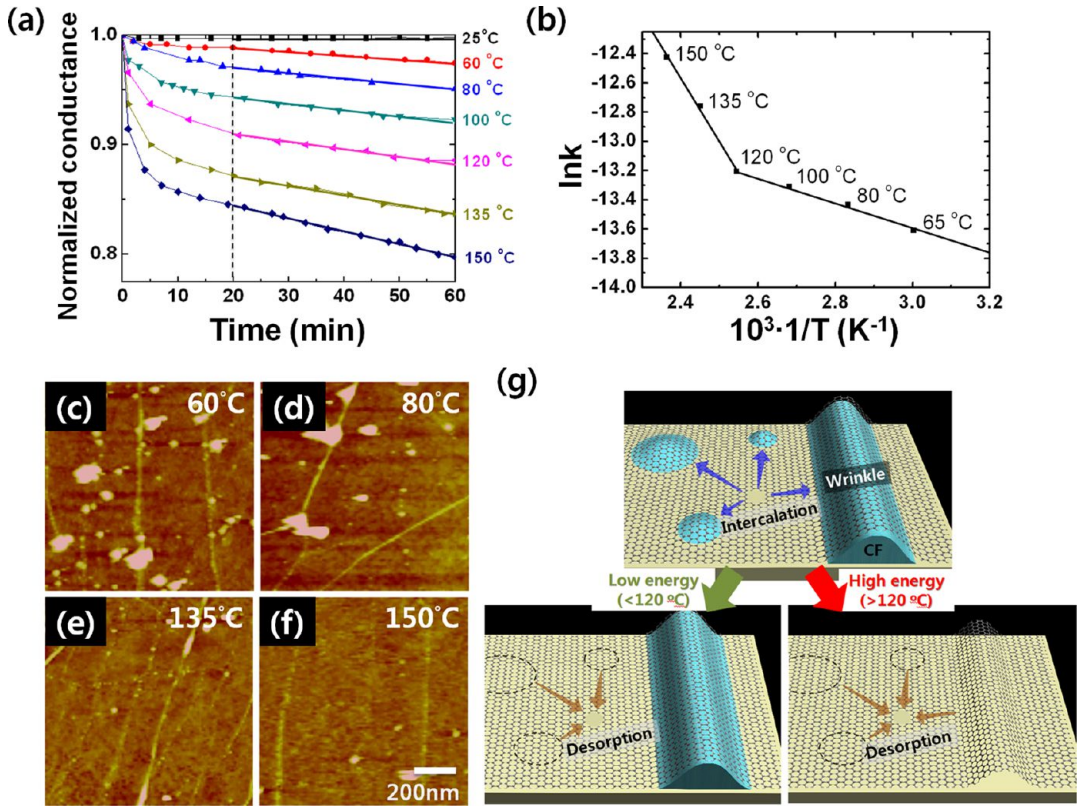

Figure 4. (a) Change in the normalized conductance as a function of time, at various annealing temperatures. (b) Arrhenius plot for the normalized conductance, where *k* represents the equilibrium rate for the change in normalized conductance. (c–f) Changes in the AFM images of the graphene surface, after annealing at (c) 60, (d) 80, (e) 135, and (f) 150 °C for 1 h. (g) Schematic illustration of the intercalation and desorption of CF.

graphene made by CF is not enough to screen the CF dipole moment.[38] The results showed that the work function of graphene was changed from 4.36 to 4.92 eV, as shown in Figure 3b. The predicted shift ($\Delta\Phi = 0.56$ eV) was qualitatively consistent with the experimental result ($\Delta\Phi = 0.58$ eV). The doping by CF can occur *via* induced dipole moments[39] rather than *via* direct charge transfer[28] because both the HOMO and LUMO levels of CF are far from the Dirac point of graphene (Supporting Information, Figure S3). When CF molecules are aligned unidirectionally with the hydrogen-upward direction, CF induces local electrostatic fields down-shifting the vacuum level, which causes p-doping, which is similar with doping by water molecules,[40] SAMs,[39] and ferroelectric material.[41] However, the calculated results showed that the Dirac point of the graphene did not move downward; this was confirmed by calculating the band structure (Supporting Information, Figure S3). The reason for this is that, theoretically, the electrons in the CF-doped graphene cannot be ejected because the calculation was conducted in a closed system. When we consider an open system, the electrons can then move through the metal electrodes and/or other metal contacts on the surface of the graphene, enabling doping to occur.

The energies for the desorption of CF molecules from intercalated sites were determined using the Arrhenius plot with the following equation:

$$E_{\text{desorption}} = -R\left[\frac{\partial \ln k}{\partial(1/T)}\right] \quad (4)$$

where R is the universal gas constant (8.314 J/mol·K) and k is the rate constant. The rate constant k for desorption of CF was determined from the equilibrium slope, that is, the conductance divided by the annealing time. Figure 4a shows the change in normalized conductance as a function of time, at various temperatures (25, 65, 80, 100, 120, 135, and 150 °C). Because the escape of adsorbed molecules induced a decrease in the conductance of the graphene, different slopes were shown as a function of annealing temperature. At room temperature, the conductance did not change with time. However, at higher annealing temperatures, the conductance decreased rapidly at short times, and then the slope leveled out, with the rate constant k becoming constant after approximately 20 min. The two different desorption energies were calculated from the Arrhenius plot (Figure 4b), 0.076 and 0.373 eV. We speculate that these two different desorption energies might have originated from the differences in the intercalated regions (*i.e.*, beneath the basal plane of the graphene and inside the wrinkles). To investigate this hypothesis, temperature-dependent AFM measurements were carried out, as shown in Figure 3c–f.

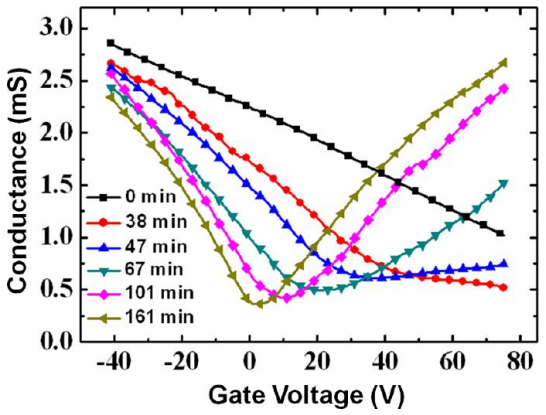

Figure 5. Gate-voltage-dependent graphene FET as a function of annealing time at 150 °C under vacuum conditions.

The temperature was varied from 25 to 150 °C, and the annealing time was fixed at 1 h. The results showed that the CF molecules adsorbed beneath the basal plane of the graphene started to become desorbed at temperatures lower than 120 °C (Figure 4c,d), whereas those in the wrinkles started to desorb from 120 °C (Figure 4e,f), as shown schematically in Figure 4g. The reason why the CF molecules intercalated in the wrinkles did not desorb easily is not obvious; however, it is likely that this phenomenon resulted from the fact that the increased contact area of the chloroform clusters in the wrinkles contributed to an enhanced interaction between the graphene and the CF molecules.

The thermal response of the conductance could be utilized to maintain certain degree of p-doping of monolayer graphene. The sample-to-sample variation of conductance of CF-doped graphene before annealing was not noticeable due to the similar quality of graphene from the same preparation methods. In addition, since rate constants associated with desorption were calculated at each temperature, the doping level could be controlled by changing desorption time. Figure 5 shows electrical measurement of a gate-voltage-dependent graphene FET as a function of annealing time at 150 °C under vacuum conditions. The result shows that Dirac voltage was changed from over 80 to 3 V. In other words, the work function of CF-doped graphene can be tuned from 5.19 to nearly 4.42 eV by controlling the degree of desorption.

CONCLUSION

In conclusion, we report stable doping of transferred graphene on the target SiO_2 substrate *via* spontaneous substrate-induced solvent intercalation. This achieves the simple, strong, stable, reproducible, controllable, low-temperature, and large-scale p-doping of graphene without sacrificing transmittance. Furthermore, we demonstrated where the CF molecules are adsorbed and how strongly they are adsorbed with the graphene. This doping method can be possibly applied to the large-area and high-performance soft electronic devices using graphene electrodes on plastic substrates.

METHODS

For the growth of monolayer graphene, copper foil was heated to 1000 °C under H_2 flowing at 10 sccm and 60 mTorr, and subsequently at 45 sccm, CH_4 gas was flowed at 300 mTorr for 30 min. The chamber was then rapidly cooled to room temperature under H_2 flowing at 10 sccm. A schematic drawing of the transfer process for CVD-grown graphene is shown in Figure S1. The CVD-grown graphene films on copper foil were covered with polymethylmethacrylate (PMMA, M_w = 340 kg mol^{-1}), and the graphene on the back side of the copper foil was removed using oxygen plasma. This sample was then floated in an aqueous solution of 0.1 M ammonium persulfate ($(NH_4)_2S_2O_8$). After all of the copper foil was etched away, the graphene film with the PMMA supporting layer was moved to a deionized water bath for 10 min, then transferred to a SiO_2 (300 nm)/Si substrate; this was followed by the removal of the PMMA support layer with acetone or chloroform (CF) for 1 h, as shown in Figure S1. To fabricate the source/drain electrodes in graphene FETs, 100 nm thick patterned gold electrodes were deposited on the graphene with a shadow mask.

The graphene films were characterized using atomic force microscopy (AFM, Digital Instruments Multimode) operating in tapping mode, Raman spectroscopy (Alpha300R, WITec, λ = 532 nm), ultraviolet photoelectron spectroscopy (8A2 beamline at the Pohang Accelerator Laboratory in Korea), UV−vis spectroscopy (Varian, CARY-5000), and characterization of the current−voltage properties of the FET devices, as measured using a Keithley 2636A semiconductor parameter analyzer under vacuum conditions.

Conflict of Interest: The authors declare no competing financial interest.

Acknowledgment. This work was supported by NRF (National Honor Scientist Program: 2010-0020414) and a grant (Code No. 2011-0031628) from the Center for Advanced Soft Electronics under the Global Frontier ResearchProgram of the Ministry of Education, Science and Technology, Korea.

Supporting Information Available: Experimental methods and additional results. This material is available free of charge *via* the Internet at http://pubs.acs.org.

REFERENCES AND NOTES

1. Lee, C.; Wei, X.; Kysar, J. W.; Hone, J. Measurement of the Elastic Properties and Intrinsic Strength of Monolayer Graphene. *Science* **2008**, *321*, 385–388.
2. Balandin, A. A. Thermal Properties of Graphene and Nanostructured Carbon Materials. *Nat. Mater.* **2011**, *10*, 569–581.
3. Blake, P.; Hill, E. W.; Castro Neto, A. H.; Novoselov, K. S.; Jiang, D.; Yang, R.; Booth, T. J.; Geim, A. K. Making Graphene Visible. *Appl. Phys. Lett.* **2007**, *91*, 063124.
4. Pedersen, T. G.; Flindt, C.; Pedersen, J.; Jauho, A.-P.; Mortensen, N. A.; Pedersen, K. Optical Properties of Graphene Antidot Lattices. *Phys. Rev. B* **2008**, *77*, 245431.
5. Lee, W. H.; Park, J.; Kim, Y.; Kim, K. S.; Hong, B. H.; Cho, K. Control of Graphene Field-Effect Transistors by Interfacial Hydrophobic Self-Assembled Monolayers. *Adv. Mater.* **2011**, *23*, 3460–3464.
6. Tan, Y. W.; Zhang, Y.; Bolotin, K.; Zhao, Y.; Adam, S.; Hwang, E. H.; Das Sarma, S.; Stormer, H. L.; Kim, P. Measurement of Scattering Rate and Minimum Conductivity in Graphene. *Phys. Rev. Lett.* **2007**, *99*, 246803.
7. Adam, S.; Hwang, E. H.; Galitski, V. M.; Das Sarma, S. A Self-Consistent Theory for Graphene Transport. *Proc. Natl. Acad. Sci. U.S.A.* **2007**, *104*, 18392–18397.

8. Castro Neto, A. H.; Guinea, F.; Peres, N. M. R.; Novoselov, K. S.; Geim, A. K. The Electronic Properties of Graphene. *Rev. Mod. Phys.* **2009**, *81*, 109.
9. Nair, R. R.; Blake, P.; Grigorenko, A. N.; Novoselov, K. S.; Booth, T. J.; Stauber, T.; Peres, N. M. R.; Geim, A. K. Fine Structure Constant Defines Visual Transparency of Graphene. *Science* **2008**, *320*, 1308.
10. Kasry, A.; Kuroda, M. A.; Martyna, G. J.; Tulevski, G. S.; Bol, A. A. Chemical Doping of Large-Area Stacked Graphene Films for Use as Transparent, Conducting Electrodes. *ACS Nano* **2010**, *4*, 3839–3844.
11. Shi, Y.; Kim, K. K.; Reina, A.; Hofmann, M.; Li, L.-J.; Kong, J. Work Function Engineering of Graphene Electrode *via* Chemical Doping. *ACS Nano* **2010**, *4*, 2689–2694.
12. Park, J.; Lee, W. H.; Huh, S.; Sim, S. H.; Kim, S. B.; Cho, K.; Hong, B. H.; Kim, K. S. Work-Function Engineering of Graphene Electrodes by Self-Assembled Monolayers for High-Performance Organic Field-Effect Transistors. *J. Phys. Chem. Lett.* **2011**, *2*, 841–845.
13. Lee, W. H.; Park, J.; Sim, S. H.; Jo, S. B.; Kim, K. S.; Hong, B. H.; Cho, K. Transparent Flexible Organic Transistors Based on Monolayer Graphene Electrodes on Plastic. *Adv. Mater.* **2011**, *23*, 1752–1756.
14. Lee, W. H.; Park, J.; Sim, S. H.; Lim, S.; Kim, K. S.; Hong, B. H.; Cho, K. Surface-Directed Molecular Assembly of Pentacene on Monolayer Graphene for High-Performance Organic Transistors. *J. Am. Chem. Soc.* **2011**, *133*, 4447–4454.
15. Lim, S.; Kang, B.; Kwak, D.; Lee, W. H.; Lim, J. A.; Cho, K. Inkjet-Printed Reduced Graphene Oxide/Poly(vinyl alcohol) Composite Electrodes for Flexible Transparent Organic Field-Effect Transistors. *J. Phys. Chem. C* **2012**, *116*, 7520–7525.
16. Gomez De Arco, L.; Zhang, Y.; Schlenker, C. W.; Ryu, K.; Thompson, M. E.; Zhou, C. Continuous, Highly Flexible, and Transparent Graphene Films by Chemical Vapor Deposition for Organic Photovoltaics. *ACS Nano* **2010**, *4*, 2865–2873.
17. Wu, J.; Agrawal, M.; Becerril, H. C. A.; Bao, Z.; Liu, Z.; Chen, Y.; Peumans, P. Organic Light-Emitting Diodes on Solution-Processed Graphene Transparent Electrodes. *ACS Nano* **2009**, *4*, 43–48.
18. Sun, T.; Wang, Z. L.; Shi, Z. J.; Ran, G. Z.; Xu, W. J.; Wang, Z. Y.; Li, Y. Z.; Dai, L.; Qin, G. G. Multilayered Graphene Used as Anode of Organic Light Emitting Devices. *Appl. Phys. Lett.* **2010**, *96*, 133301.
19. Wei, D.; Liu, Y.; Wang, Y.; Zhang, H.; Huang, L.; Yu, G. Synthesis of N-Doped Graphene by Chemical Vapor Deposition and Its Electrical Properties. *Nano Lett.* **2009**, *9*, 1752–1758.
20. Das, A.; Pisana, S.; Chakraborty, B.; Piscanec, S.; Saha, S. K.; Waghmare, U. V.; Novoselov, K. S.; Krishnamurthy, H. R.; Geim, A. K.; Ferrari, A. C.; *et al.* Monitoring Dopants by Raman Scattering in an Electrochemically Top-Gated Graphene Transistor. *Nat. Nanotechnol.* **2008**, *3*, 210–215.
21. Dong, X.; Fu, D.; Fang, W.; Shi, Y.; Chen, P.; Li, L.-J. Doping Single-Layer Graphene with Aromatic Molecules. *Small* **2009**, *5*, 1422–1426.
22. Park, J.; Jo, S. B.; Yu, Y.-J.; Kim, Y.; Yang, J. W.; Lee, W. H.; Kim, H. H.; Hong, B. H.; Kim, P.; Cho, K.; *et al.* Single-Gate Bandgap Opening of Bilayer Graphene by Dual Molecular Doping. *Adv. Mater.* **2012**, *24*, 407–411.
23. Chen, W.; Chen, S.; Dong, C. Q.; Xing, Y. G.; Wee, A. T. S. Surface Transfer p-Type Doping of Epitaxial Graphene. *J. Am. Chem. Soc.* **2007**, *129*, 10418–10422.
24. Medina, H.; Lin, Y. C.; Obergfell, D.; Chiu, P. W. Tuning of Charge Densities in Graphene by Molecule Doping. *Adv. Funct. Mater.* **2011**, *21*, 2687–2692.
25. Lee, W. H.; Suk, J. W.; Lee, J.; Hao, Y.; Park, J.; Yang, J. W.; Ha, H.-W.; Murali, S.; Chou, H.; Akinwande, D.; *et al.* Simultaneous Transfer and Doping of CVD-Grown Graphene by Fluoropolymer for Transparent Conductive Films on Plastic. *ACS Nano* **2012**, *6*, 1284–1290.
26. Santos, J. E.; Peres, N. M. R.; Lopes dos Santos, J. M. B.; Castro Neto, A. H. Electronic Doping of Graphene by Deposited Transition Metal Atoms. *Phys. Rev. B* **2011**, *84*, 085430.
27. Wang, X.; Xu, J.-B.; Xie, W.; Du, J. Quantitative Analysis of Graphene Doping by Organic Molecular Charge Transfer. *J. Phys. Chem. C* **2011**, *115*, 7596–7602.
28. Chen, W.; Chen, S.; Qi, D. C.; Gao, X. Y.; Wee, A. T. S. Surface Transfer p-Type Doping of Epitaxial Graphene. *J. Am. Chem. Soc.* **2007**, *129*, 10418–10422.
29. Klar, P.; Casiraghi, C. Raman Spectroscopy of Graphene in Different Dielectric Solvents. *Phys. Status Solidi C* **2010**, *7*, 2735–2738.
30. Bae, S.; Kim, S. J.; Shin, D.; Ahn, J.-H.; Hong, B. H. Towards Industrial Applications of Graphene Electrodes. *Phys. Scr.* **2012**, *2012*, 014024.
31. Shin, H. J.; Choi, W. M.; Choi, D.; Han, G. H.; Yoon, S. M.; Park, H. K.; Kim, S. W.; Jin, Y. W.; Lee, S. Y.; Kim, J. M.; *et al.* Control of Electronic Structure of Graphene by Various Dopants and Their Effects on a Nanogenerator. *J. Am. Chem. Soc.* **2010**, *132*, 15603–15609.
32. Nolen, C. M.; Denina, G.; Teweldebrhan, D.; Bhanu, B.; Balandin, A. A. High-Throughput Large-Area Automated Identification and Quality Control of Graphene and Few-Layer Graphene Films. *ACS Nano* **2011**, *5*, 914–922.
33. Li, X.; Cai, W.; An, J.; Kim, S.; Nah, J.; Yang, D.; Piner, R.; Velamakanni, A.; Jung, I.; Tutuc, E.; *et al.* Large-Area Synthesis of High-Quality and Uniform Graphene Films on Copper Foils. *Science* **2009**, *324*, 1312–1314.
34. Pisana, S.; Lazzeri, M.; Casiraghi, C.; Novoselov, K. S.; Geim, A. K.; Ferrari, A. C.; Mauri, F. Breakdown of the Adiabatic Born–Oppenheimer Approximation in Graphene. *Nat. Mater.* **2007**, *6*, 198–201.
35. Yu, D.; Yang, Y.; Durstock, M.; Baek, J.-B.; Dai, L. Soluble P3HT-Grafted Graphene for Efficient Bilayer–Heterojunction Photovoltaic Devices. *ACS Nano* **2010**, *4*, 5633–5640.
36. Zhang, Y.; Brar, V. W.; Wang, F.; Girit, C.; Yayon, Y.; Panlasigui, M.; Zettl, A.; Crommie, M. F. Giant Phonon-Induced Conductance in Scanning Tunnelling Spectroscopy of Gate-Tunable Graphene. *Nat. Phys.* **2008**, *4*, 627–630.
37. Goumans, T. P. M.; Wander, A.; Brown, W. A.; Catlow, C. R. A. Structure and Stability of the (001) Alpha-Quartz Surface. *Phys. Chem. Chem. Phys.* **2007**, *9*, 2146–2152.
38. DiVincenzo, D. P.; Mele, E. J. Self-Consistent Effective-Mass Theory for Intralayer Screening in Graphite Intercalation Compounds. *Phys. Rev. B* **1984**, *29*, 1685–1694.
39. Yokota, K.; Takai, K.; Enoki, T. Carrier Control of Graphene Driven by the Proximity Effect of Functionalized Self-Assembled Monolayers. *Nano Lett.* **2011**, *11*, 3669–3675.
40. Yavari, F.; Kritzinger, C.; Gaire, C.; Song, L.; Gulapalli, H.; Borca-Tasciuc, T.; Ajayan, P. M.; Koratkar, N. Tunable Bandgap in Graphene by the Controlled Adsorption of Water Molecules. *Small* **2010**, *6*, 2535–2538.
41. Zheng, Y.; Ni, G.-X.; Toh, C.-T.; Tan, C.-Y.; Yao, K.; Özyilmaz, B. Graphene Field-Effect Transistors with Ferroelectric Gating. *Phys. Rev. Lett.* **2010**, *105*, 166602.